Kinetic critical radius in nucleation and growth processes - Trapping effect

Z. Erdélyi, Z. Balogh, D.L. Beke

Department of Solid State Physics, University of Debrecen, P. O. Box 2, H-4010 Debrecen, Hungary

Abstract

The critical nucleus size—above which nuclei grow, below dissolve—during diffusion controlled nucleation in binary solid-solid phase transformation process is calculated using kinetic Monte Carlo. If atomic jumps are slower in an A-rich nucleus than in the embedding B-rich matrix, the nucleus traps the A atoms approaching its surface. It has not enough time to eject A atoms before new ones arrive, even if it would be favourable thermodynamically. In this case the critical nucleus size can be even by an order of magnitude smaller than expected from equilibrium thermodynamics or without trapping.

Keywords: homogeneous nucleation of phase transformations, phase transformation kinetics, Monte Carlo techniques

1. Introduction

Thousands of studies probing the nucleation and growth processes of incommensurate materials or using the classical nucleation theory to interpret the results have been published in the last years [1]. This is because the fabrication of many novel materials requires the ability to exercise precise control over the growth of precipitates in a host material or in thin films on a host substrate or of precipitates in a host [2, 3], in crystallisation processes [4], in preparation of nanoparticles [5, 6], in isothermal austenite decomposition in nearly eutectoid steel [7], etc. Accordingly, also the theory itself has been discussed a lot (e.g. three ways of implementing classical nucleation and growth theories was presented and discussed recently in Ref. 8, 9)

According to the classical (thermodynamic) "nucleation and growth" theory [10, 11] of phase transformation process, there exists a critical nucleus size or an n_c critical number of atoms (or molecules, ions, etc.) being in the nucleus. The nuclei containing atoms less than n_c dissolve into the matrix, whereas the larger ones grow continuously. This can be obtained from simple considerations on the radius dependence of the free energy of a nucleus (see e.g. Ref. 12). The equation, describing the energy gain and loss of the system when a nucleus is created, contains two terms, the chemical energy gain and surface energy loss. For instance in the case of creation of an A-rich nucleus (in a B-rich matrix) the energy gain arises from the elimination of the higher energy $A - B$ heteroatomic bonds for the benefit of

the lower-energy $A - A$ or $B - B$ homoatomic bonds. This gain is proportional to the volume (or to n_{vol}, the number of atoms in the volume of the nucleus). The energy loss originates from the creation of the nucleus/matrix interface; the number of atoms being at the interface (n_{int}) is obviously proportional to the surface of the nucleus. Thus the sum of these two terms is not a monotonic function of the size (n) but has a maximum, determining n_c. According to this phenomenological picture, below n_c a small increase in n increases, while above n_c decreases the energy of a nucleus.

From kinetic aspects, nucleation is known to occur by formation of atomic clusters of various sizes (see e.g. Refs. 13, 14). The cluster size changes randomly as a result of successive attachments and detachments of single atoms to and from the cluster. As atomic attachments and detachments are random events, a given n-sized cluster can decay or grow and reach a macroscopic size with a certain probability. There exists a particular cluster size $n = n^*$ when atoms are attached and detached to and from the cluster with equal frequency, i.e. the $P(n = n^*)$ growth probability of the cluster is $1/2$. Clusters of size $n < n^*$ tend to decay, i.e. $P(n < n^*) < 1/2$, because per unit time less molecules are attached to than detached from them. On the contrary, the clusters of size $n > n^*$ are characterised by attachment frequencies greater than the detachment ones and for that reason these clusters tend to grow up to macroscopic sizes, i.e. $P(n > n^*) > 1/2$.

In principle, there is no reason for supposing that the thermodynamically defined n_c, called as "thermodynamic critical size", and the kinetically defined n^*, called as "kinetic criti-

Email address: `zerdelyi@dragon.unideb.hu` (Z. Erdélyi)
URL: `http://dragon.unideb.hu/~zerdelyi` (Z. Erdélyi)

Table 1: Examples of self and impurity diffusion data for Fe-Cr and Cu-Co binary systems [16]. The columns are the pre-exponential factor, the activation energy and the diffusion coefficient calculated for 800 K, respectively. The footnote shows the calculated values of m' (see also the text).

	D_0 $(10^{-4}\ \mathrm{m^2/s})$	Q (kJ/mol)	**D** $(\mathrm{m^2/s})$
Fe-Cr[a]			
Fe in Fe	2.01	240.7	$\mathbf{3.86 \times 10^{-20}}$
Cr in Fe	8.52	250.8	$\mathbf{3.58 \times 10^{-20}}$
Cr in Cr	1.6	339.1	$\mathbf{1.15 \times 10^{-26}}$
Fe in Cr	0.47	332	$\mathbf{9.86 \times 10^{-27}}$
Cu-Co[b]			
Cu in Cu	0.35	203.6	$\mathbf{1.78 \times 10^{-18}}$
Co in Cu	0.43	214.3	$\mathbf{4.37 \times 10^{-19}}$
Co in Co	0.55	288.5	$\mathbf{7.99 \times 10^{-24}}$
Cu in Co	1	275	$\mathbf{1.11 \times 10^{-22}}$

[a]$m'_{Fe} = \log_{10} \frac{D_{\mathrm{FeinFe}}}{D_{\mathrm{FeinCr}}} = 6.59; \quad m'_{Cr} = \log_{10} \frac{D_{\mathrm{CrinFe}}}{D_{\mathrm{CrinCr}}} = 6.49$

[b]$m'_{Cu} = \log_{10} \frac{D_{\mathrm{CuinCu}}}{D_{\mathrm{CuinCo}}} = 4.21; \quad m'_{Co} = \log_{10} \frac{D_{\mathrm{CoinCu}}}{D_{\mathrm{CoinCo}}} = 4.74$

cal size" are identical. For example Nishioka showed analytically for a single-component system that n_c may be somewhat smaller than n^* [15]. For example for water nucleation from vapour this difference is 1%.

In this paper, based on kinetic Monte Carlo calculations of nucleation and growth processes *in binary solids*, we demonstrate that if the atomic jumps are orders of magnitude slower in the nucleus than in the embedding matrix, the kinetic critical nucleus size can be even by *an order of magnitude smaller* than otherwise (when the atomic jumps are equal in the nucleus and in the matrix, or the jumps are faster in the nucleus). Since, if for instance the $A-A$ bonds are much stronger than the $A-B$ and $B-B$ ones, an A atom jumps frequently in the B (rich) matrix but after attaching to the A (rich) nucleus can hardly jump any more. Practically the nucleus traps the A atoms approaching its surface. Therefore, we show that a kinetic parameter drastically influences n^* and so also its deviation from n_c in binary solids.

Besides its theoretical importance, our finding can have practical interest in crystallization processes (see e.g. Ref. 4) or in diffusion controlled solid state transformations (e.g. quenching and phase separation; precipitation) of supersaturated solid solutions, which is an important step in many technological procedures.

2. Theory

The ratio of the atomic jump probabilities or diffusion coefficients in the nucleus and in the matrix is several orders of magnitude in real systems (see e.g. Table 1 and Ref. 16), and originates from the difference in the bonding strength. Therefore, the jump probabilities of the atoms depends on the local environment, i.e. on the *local composition*.

It is very common in the diffusion literature to describe the composition dependence of the diffusion coefficients by an exponential function [16]. This is also in accordance with the

form of composition dependence of the jump probabilities in kinetic Monte Carlo (see Appendix Appendix A) and the jump frequencies in kinetic mean field models [17], where the activation energies of the jump frequencies depend linearly on the composition in a homogeneous alloy (see Appendix Appendix B).

In principle one has to distinguish between the (tracer) diffusion coefficients of A and B atoms: $D_A = D_A^0 \exp(m_A c_A)$ and $D_B = D_B^0 \exp(m_B c_B)$, where D_A^0 as well as D_B^0 are composition independent factors, c_A is the composition of the A atoms, m_A and m_B are parameters determining the strength of the composition dependence. It is worth introducing the $m'_A = m_A \log_{10} e$ and $m'_B = m_B \log_{10} e$ parameters (e is the base of natural logarithm), which give in orders of magnitude the ratios of the diffusion coefficients in the pure A and B matrixes. For instance, $m'_A = 4$ means that the A atoms jumps $10,000$ times faster in the A matrix than in the B. Accordingly, m'_A and m'_B parameters can be obtained form the ratio of the corresponding diffusion coefficients as shown in Table 1 (and can also be called as diffusion asymmetry parameters) [18].

Taking into account that $m'_{Fe} \cong m'_{Cr}$ and $m'_{Cu} \cong m'_{Co}$ in Table 1, we assumed in our investigations that the diffusion coefficients have identical composition dependence, i.e. $m'_A = m'_B \equiv m'$. Of course, this does not mean that $D_A = D_B$, since $D_A^0 \neq D_B^0$ in general.

It can also be seen from Table 1 that a ratio of four to eight orders of magnitude of the diffusivities/jump probabilities in the nucleus and in the matrix are not unrealistic values, especially for low temperature experiments. For example at 800 K, $m' \cong 6.5$ in Fe-Cr, $m' \cong 4.5$ in Cu-Co systems (see also some other examples and interesting phenomena related to the large asymmetry in Ref. 19, 20, 21, 22, 23, 24). Note, that according to the Arrhenius-type temperature dependence of the diffusion coefficient, m' increases with decreasing temperature due to the different activation energies in A and B. As a final remark, m' can also be calculated from the difference in the $A-A$ and $B-B$ pair interaction energies (see e.g. Ref. 18 and Appendix Appendix A).

In the following, we show how m' influences the critical nucleus size in a supersaturated phase separating $A-B$ alloy (from now on, the 'critical size' and the 'critical nucleus size' mean always the kinetic ones if it is not stated otherwise). In principle, two cases should be considered: positive (the jumps are faster in the matrix) and negative (the jumps are slower in the matrix) values of m'. However, since for $m' < 0$ values we found that the critical nucleus size was independent of m', only the results of the calculations performed for $m' \geq 0$, i.e. when the atomic jumps are faster in the matrix, are described in details. In this case significant change in the critical size versus m' was observed.

One dimensional kinetic mean filed (KMF) and three dimensional kinetic Monte Carlo (KMC) models (see Ref. 25, 26, 17 and the Appendixes for more information on the models) were used to study how m' influences the critical nucleus size. Although the KMF is deterministic and limited to one dimension, and its results cannot be exactly compared to that of KMC, in order to save time we used the KMF to map roughly the ade-

quate range of input parameters and the expectable tendencies. Then, with each chosen input parameter set we run the KMC several times.

The temperature and the regular solid solution parameter (proportional to the mixing energy; see Appendixes for detailed information) were chosen to be $T = 800$ K and $V = 0.025$ eV, respectively. These parameters correspond e.g. to the fcc Cu-Co [27, 28] system, at $T/T_c \approx 0.51$, where T_c is the maximum temperature of the miscibility gap; and to the bcc Fe-Cr [29, 30, 31] like system, at $T/Tc \approx 0.73$. m' was varied between -4 and 8 in our calculations.

It is worth mentioning that the ratio of the diffusivities can also be very different from unity in crystallisation processes, when solid nuclei are in a "liquid matrix". Thus the trapping effect may play important role here, too.

3. Results and Discussion

3.1. Homogeneous matrix

As a first step nucleation from a homogeneous supersaturated solid solution was studied. To avoid the spinodal decomposition, the initially homogeneous matrix was supersaturated but its composition was outside the spinoda. After some estimations and numerous KMC test runs, the composition of minority (A) atoms in the matrix was chosen to be 17%.

We counted the number of A atoms in each nucleus (see Appendixes for a detailed description of the evaluation process) and plotted, from time to time, the P_n nucleus size distribution (related to the number density of nuclei) on a log-log scale; for better statistics, we summed the results of 3 KMC runs (Fig. 1). One can distinguish two regimes in the graph, a faster and a slower decaying part.

The faster decaying part, left hand side of the distribution curve, corresponds to the sub-critical sized, unstable nucleus—*embryos*—existing in the solid solution. These embryos appear and dissolve continuously, forming an embryos-solid solution system being in dynamic equilibrium. This part of the curve is characterised by a power function with a cutoff, n_{cut}: $P_n \propto n^{-\alpha} \exp(-n/n_{cut})$. The position of the cutoff is determined by the current composition of the solid solution matrix.

If the size of an embryo in the solid solution becomes larger than the critical nucleus size, the nucleus absorbs A atoms from the matrix and grows continuously. The super-critical sized, continuously growing, stable nuclei—*precipitates*—form the slower decaying, right hand side of the curve in Fig. 1.

With time, more and more precipitates appear, meanwhile the existing ones grow further (shift to the right in the plot). Consequently, the concentration of the solid solution and also the cutoff value decreases (shifts to the left). At a certain point, the cutoff value will be smaller than the critical nucleus size, thus no new precipitates will appear. Since the size of the precipitates increases with time, a gap will be formed between the two parts of the distribution curve in Fig. 1.

The position (lower and upper limits) of the gap and the number of stable precipitates are related to the critical nucleus size. The critical nucleus size is in the gap; the higher the number
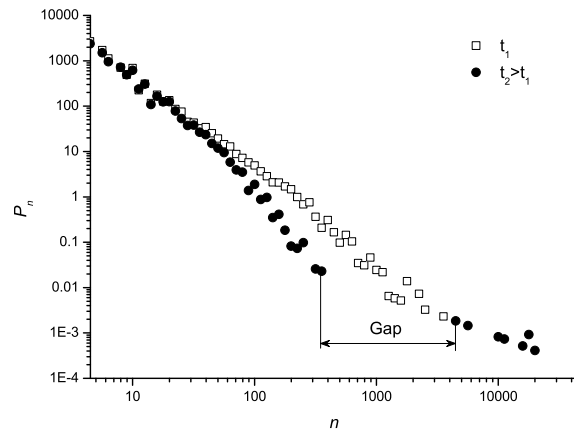

Figure 1: Nucleus size distribution function for $m' = 0$. The hollow squares represent an earlier stage. The filed circles show a more developed state, where a gap between the embryos of the solid solution and the precipitates was formed.
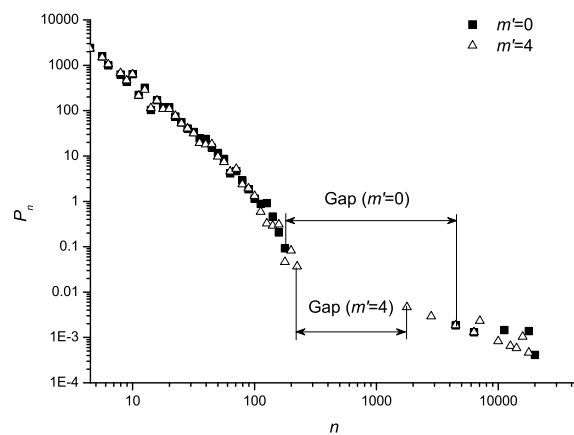

Figure 2: Nucleus site distribution functions for $m' = 0$ and $m' = 4$. Although the embedding matrixes are practically identical, the size distributions of the precipitates differ. The precipitates are smaller and more numerous in case of $m' = 4$ than in case of $m' = 0$.

of the precipitates is, the smaller the critical nucleus size is. Consequently, for different critical nucleus sizes the distribution functions look different.

Fig. 2 shows the distribution functions for two cases, when the atomic jums are faster in the matrix than in the nucleus ($m' = 4$) and when they are identical ($m' = 0$). The parts describing the solid solution are practically identical for both cases, however, the other parts, corresponding to the precipitates, are different. This shows clearly that the size distributions of the precipitates differ, although the embedding matrixes are identical. In case of $m' = 4$, the smallest precipitates consist of more than 4400 A atoms, whereas in case of $m' = 0$ the smallest precipitates contain less than 1800 A atoms. The number of precipitates is also different: e.g. 8 for $m' = 0$; and 12 for $m' = 4$ in a $100 \times 100 \times 100$ box. This, approximately 50%, difference remains throughout the later ripening stage. Thus when the atomic jumps are faster in the nucleus than in the embedding matrix, smaller and more numerous precipitates are expected.
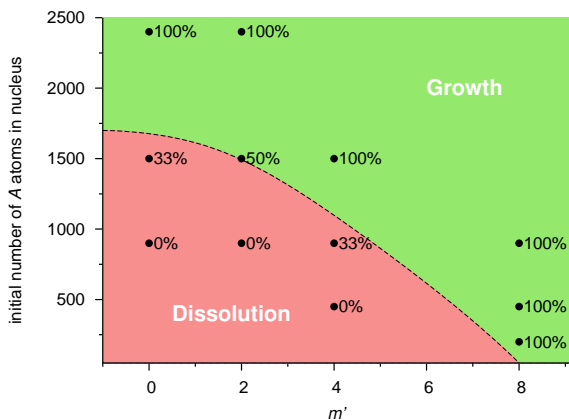
Figure 3: Nuclei size – m' map. The black squares show the initial size of the nuclei and the numbers give the probability of growth. The dashed curve at the border of the red and green areas corresponds to the estimated 50% probability of growth, i.e. to the critical nucleus size. The green area corresponds to super-critical while the red to sub-critical nuclei, respectively.
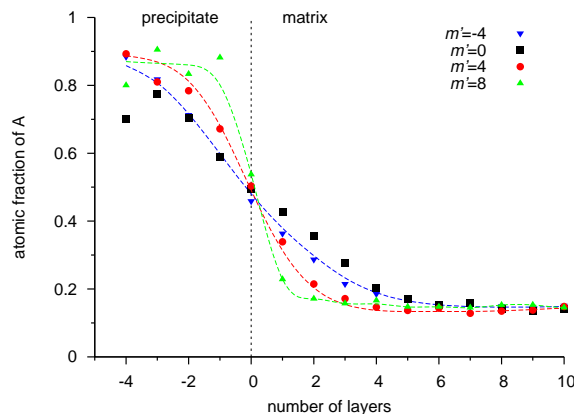

Figure 5: Radial distribution functions of similar sized growing nuclei calculated with different asymmetry parameter, m'. It can be seen that for $m' = 0$ symmetrical case the interface is rather wide. For positive m' the interface width decreases with the asymmetry, while the negative m' has no effect on it. (The dashed lines are only to guide the eyes.)

3.2. Single nucleus

For a deeper understanding of the processes, we also investigated the behaviour of a single spherical nucleus put into a homogeneous solid solution matrix. The initial size of the nucleus was varied to find the critical nucleus depending on m'. The nucleus contained $200-3200$ atoms initially and m' was chosen to be 0, 2, 4, 8. Initially 85% of the atoms was A and 15% was B in the nucleus. Whereas in the matrix 15% of the atoms was A and 85% was B. These compositions correspond approximately to the composition of the spontaneously growing precipitates and to the concentration of the matrix after the gap formation, respectively. Thus the probability of spontaneous precipitate formation is very low. This allowed us to investigate the critical nucleus size under similar conditions as in the spontaneous formation case but without any interaction between large precipitates.

Figure 3 summarises the results of the calculations. It can be seen, as expected from thermodynamics, that for $m' = 0$ the nuclei with super-critical size grow, whereas the sub-critical ones dissolve (Fig. 4). Furthermore, there is a size range, around the critical size, where the nucleus may either grow or dissolve due to the stochastic processes. If the random motion of the A atoms in the matrix leads to temporary enrichment or depletion of the matrix in the vicinity of the nucleus, then it grows or shrinks, respectively. The growth/dissolution ratio is equal to 0.5 for the exact critical size, otherwise differs from 0.5, proportionally how the current nucleus size deviates from the critical one. Obviously around 0.5 the nucleus "hesitates" to grow or to dissolve. This means that before the nucleus dissolves completely or starts to grow definitely its size may fluctuate.

Figure 3 also clearly shows that the border between the growth and dissolution ranges shifts towards smaller nucleus sizes with increasing m'.

Figure 5 shows another interesting consequence of the trapping effect. As can be seen in the radial distribution functions of three growing precipitates, calculated for $m = 0, 4$ and 8, sharper precipitate/matrix interface belongs to larger m'. This

can also be observed visually in 3D images of the nuclei in Fig. 6. On the other hand, the shape of the interface is the same for $m' = 0$ and $m' = -4$. We have also checked that after very long time the shape of the interfaces in all cases (i.e. for $m > 0$ values, too) was similar to those obtained for $m' = 0$, which can be called as the equilibrium shape.

Regarding the interpretation of the phenomena observed, first, one has to understand why the obtained critical size is smaller for positive m' values (fast diffusion in the matrix, slow diffusion in the nucleus). The explanation is plausible: An A atom jumps frequently in the B matrix but after attaching to the A (rich) nucleus cannot jump for relatively long time. Practically the nucleus traps the A atom. The nucleus does not have enough time to eject A atoms before new ones arrive, even if the size of the nucleus is smaller than the critical size calculated form thermodynamic considerations, and so the free energy of the nucleus increases. After the size of the nucleus exceeds the "thermodynamic critical size", thermodynamics also assists the growth process. Obviously, the trapping is much stronger for larger m' (larger difference in the $A - A$ and $B - B$ pair interaction energies), thus the "kinetic critical size" deviates more from the "thermodynamic critical size", even by one order of magnitude for realistic values of m'.

For similar reason, the shape of the interface is different from the equilibrium one for $m' > 0$: The system practically do not have enough time to reach the local equilibrium [33] (see Fig. 5). The formation of the "equilibrium shape" of the interface would require fast rearrangements of atoms at the nucleus/matrix interface. However, inside the nucleus the jump probabilities are much lower, disallowing the fast rearrangements of atoms.

If $m = 0$, an A atom in the B matrix jumps as frequently as in the nucleus. Thus after attaching to the nucleus its jump rate does not change. Consequently, the rearrangement of the atoms at the interface takes place on the same time scale as new A atoms arrive. Thus, in the interface region the local equilibrium can be reached continuously. For $m < 0$, the jump frequencies
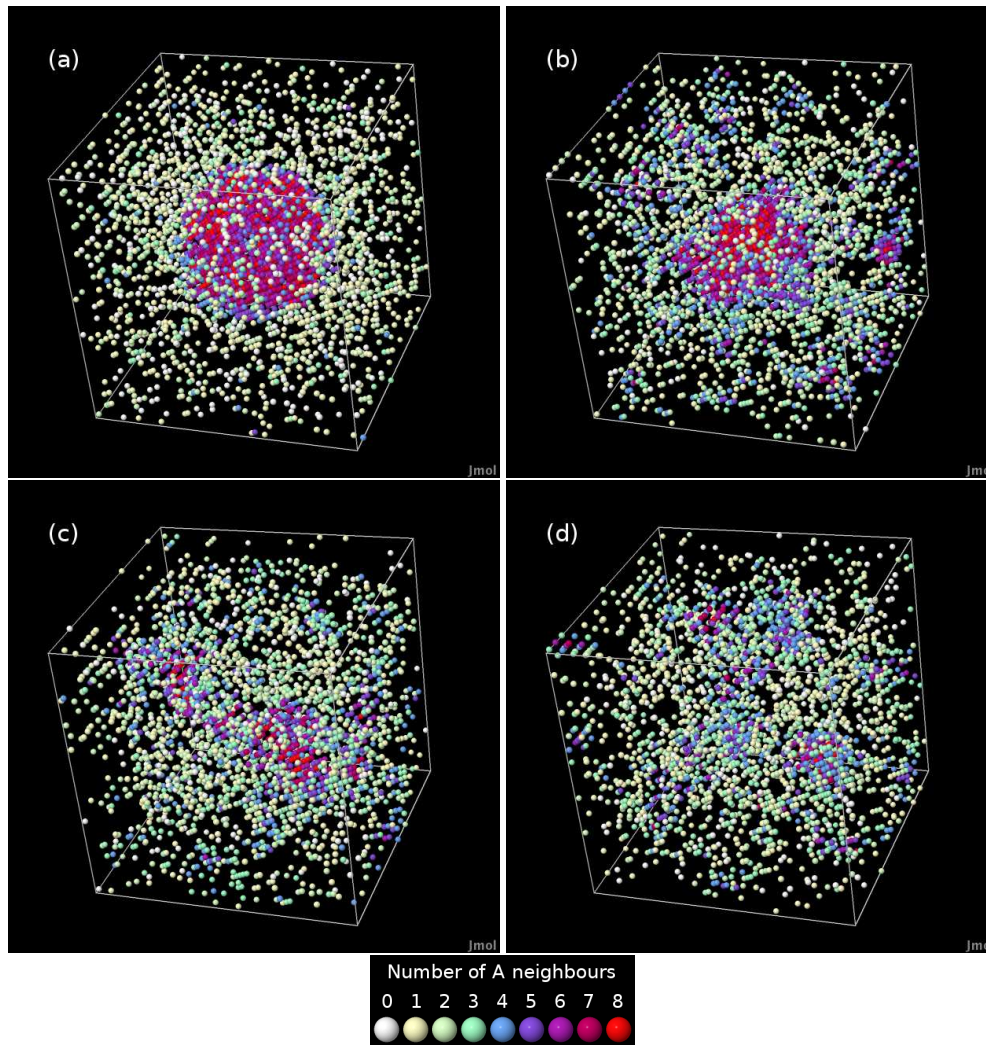
Figure 4: Sequence of 3D images of a nucleus during a dissolution process $m' = 0$. Only the *A* atoms are plotted. The colour scale illustrates how many *A* neighbours has an *A* atom. (a) initial nucleus; (b) the nucleus shrinks and some small, unstable *A*-rich nuclei (embryos) forms in the matrix; (c) the nucleus is practically dissolved; (d) later on only some unstable *A*-rich nuclei (embryos) can be observed. (only a small part of the KMC cell, around the dissolving nucleus, is plotted) [32]
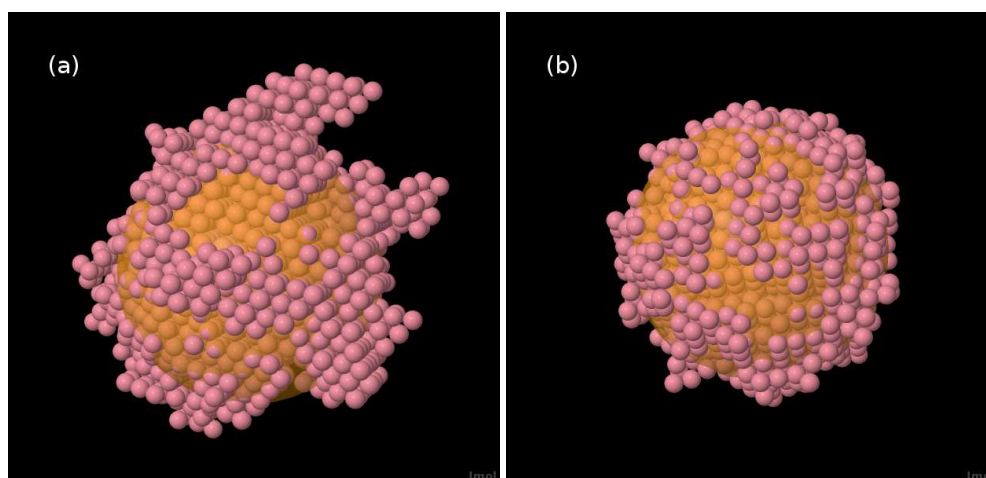

Figure 6: The figures show the morphology of precipitates after a growth of 10% for (a) $m' = 0$ and (b) $m' = 8$. The initial nucleus – translucent orange sphere – consisted of 1679 minority (*A*) atoms in both cases. Now they consist of (a) 1846 and (b) 1845 minority atoms. The precipitate (b) is much more compact than the (a) one of which surface is much rougher (there are not only crests on the sphere surface but also valleys underneath). [32]

are much faster in the *A* (rich) nucleus than in the *B* (rich) matrix. Consequently, the attached *A* atom has enough time (even more than in case of $m' = 0$) either to go inside the nucleus and form the local equilibrium or to escape from the nucleus until new *A* atoms arrive. Thus, the whole nucleus, and also the interface region can continuously be in local equilibrium.

It is also worth mentioning that in the framework of the classical model of nucleation and growth the interface energy is a very important input parameter determining the critical radius [11, 12], because they are proportional to each other. There is long standing debate in the literature [12] about the proper value of the interface energy and estimations of the critical radius (or the interface energy from the critical radius). If the diffusion is much faster in the matrix than in the nucleus, these estimations can contain considerable errors, because the kinetic critical radius can be even an order of magnitude less than otherwise (or the equilibrium critical radius). In addition, in this case the shape and thus the energy of the interface can also be different from the equilibrium one.

4. Conclusions

In this paper, we have shown that if the atomic jumps are slower in the *A*-rich nucleus nucleus than in the *B*-rich embedding matrix, peculiar behaviour is observed. With the increase of the ratio of the jump probabilities in the matrix and in the nucleus, the kinetic critical nucleus size—for which the growth probability is 1/2—may decrease by an order of magnitude. The origin of this effect is that the *A*-rich nuclei trap the attaching *A* atoms. The nuclei do not have enough time to eject *A* atoms before new ones arrive, even if their size is smaller than the thermodynamic critical size, and thus the ejection would be favourable thermodynamically. When the diffusion is the same in the matrix and the nucleus or if it is faster in the nucleus, such effects were not observed.

Acknowledgments

Appendixes

Appendix A. Three dimensional kinetic Monte Carlo model (KMC)

Monte Carlo simulations of the kinetic process were performed using the residence-time algorithm [26]. The simulation box contained ($L_x \times L_y \times L_z$) sites in body and face centered cubic (BCC and FCC, respectively) structures with periodic boundary conditions. Typically, $100 \times 100 \times 100$ boxes (one million atoms) were used but larger and smaller $L_x \neq L_y \neq L_z$ boxes were also used to test the independency of the results from the box size and geometry. As there was always one vacancy in the simulation box, the vacancy concentration was proportional to the box

size. Thus, by changing the box size, not only the size independence but also the vacancy concentration independence of the results were checked. Furthermore, we note that for comparison to real time scale, our simulation time should be rescaled to corresponding real concentrations.

If only atom-vacancy exchange is allowed, the exchange probability of a vacancy-atom pair can be calculated from the binding energy of the atom. This energy can be calculated easily in a simple nearest-neighbour interaction approximation either for an *A* (E_A) or *B* (E_B) atom:

$$
\begin{aligned}
E_A &= n_A V_{AA} + n_B V_{AB}, \\
E_B &= n_A V_{AB} + n_B V_{BB},
\end{aligned} \tag{A.1}
$$

where n_A and n_B are the number of *A* and *B* atoms in the vicinity of the given atom, V_{ij} ($i, j = A$ or B) is the interaction energy between an ij atom pair. Introducing $V = V_{AB} - \frac{V_{AA}+V_{BB}}{2}$ and $M = \frac{V_{AA}-V_{BB}}{2}$, Eqs. (A.1) can be written as:

$$
\begin{aligned}
E_A &= -n_A(V - M) + n V_{AB}, \\
E_B &= -(n - n_A)(V + M) + n V_{AB}.
\end{aligned}
$$

where $n = n_A + n_B$ is the number of neighbors of an atom, V, is the regular solid solution parameter [proportional to the mixing energy and measures the phase separating ($V > 0$) or ordering ($V < 0$) tendency] and M measures the diffusion asymmetry ($m' = -2nM/kT \log_{10} e$, where e is the base of natural logarithm) [25]. Using the usual Arrhenius- relationship between the activation energy ($Q_i = E^0 - E_i$, where E^0 is the saddle point energy, and $i = A, B$) and the probability [$\Gamma_{iV} = \nu \exp(-Q_i/kT)$], the exchange probabilities of a vacancy-*i* atom pair are:

$$
\begin{aligned}
\Gamma_{VA} &= \nu \exp\left[-\frac{\hat{E}^0 + n_A(V - M)}{kT}\right], \\
\Gamma_{VB} &= \nu \exp\left[-\frac{\hat{E}^0 + (n - n_A)(V + M)}{kT}\right],
\end{aligned}
$$

where k and T are the Botzmann's constant and the absolute temperature, ν is the attempt frequency, and $\hat{E}^0 = -E^0 + n V_{AB}$. $\hat{E}^0$ is taken to be constant for a given system, and thus it may be set to zero during calculations (but can be considered in the time scaling if needed). Note that $\Gamma_{VA} \neq \Gamma_{VB}$ in a pure *B* matrix. This means that–as the jump probability is proportional to the diffusion coefficient–$D_A^0 \neq D_B^0$.

It is worth noting that in a one-vacancy KMC calculation the vacancy concentration is defined by the finding probability of the vacancy in a small volume. (This definition is also valid even in a multi-vacancy model, since in case of dilute vacancy concentration the probability to find more than one vacancy in a small volume is negligible.) It is obvious that if the exchange probability of the vacancy and an *i* atom pair is larger e.g. in the *B* (rich) matrix than in the *A* (rich) nucleus, the finding probability of a vacancy in the *B* matrix is also larger than in the

A nucleus. This shows that the faster diffusion in the *B* matrix originates not only from the faster exchange of a vacancy-*i* atom pair but also form that the vacancy is in the *B* matrix more frequently than in the *A* nucleus, i.e. the vacancy concentration is larger in the *B* matrix than in the nucleus.

Appendix B. One dimensional kinetic mean filed model (KMF)

Our model to calculate the time evolution of the composition on a one-dimensional lattice is based on Martin's equations [17]. However, we use our own composition dependent activation barriers (diffusion asymmetry) in the exchange frequencies, which unify the advantages of other barriers used in the literature as was shown in Ref. 25.

The net flux of A atoms from plane *i* to $(i + 1)$ is given by

$$J_{i,i+1} = z_v \left[c_i(1 - c_{i+1})\Gamma_{i,i+1} - c_{i+1}(1 - c_i)\Gamma_{i+1,i} \right],$$

where c_i is the atomic fraction of *A* atoms in plane *i*, $\Gamma_{i,i+1}$ is the frequency with which an *A* atom in plane *i* exchanges with a *B* atom in plane $i + 1$ and z_v is the vertical coordination number. It is usually assumed that the exchange frequencies have an Arrhenius type temperature dependence:

$$\Gamma_{i,i+1} = \Gamma_i \gamma_i \quad \text{and} \quad \Gamma_{i+1,i} = \Gamma_i / \gamma_i$$

with

$$\Gamma_i = \Gamma_0 \exp[\alpha_i/kT] \quad \text{and} \quad \gamma_i = \exp[-\varepsilon_i/kT],$$

were $\Gamma_0 = \nu \exp[-\hat{E}_0/kT]$, ν denotes the attempt frequency, $\hat{E}_0$ is composition independent and contains the saddle point energy, *k* is the Boltzmann constant, *T* is the absolute temperature, and

$$\alpha_i = [z_v(c_{i-1} + c_{i+1} + c_i + c_{i+2}) + z_l(c_i + c_{i+1})] M$$

as well as

$$\varepsilon_i = [z_v(c_{i-1} + c_{i+1} - c_i - c_{i+2}) + z_l(c_i - c_{i+1})] V.$$

Here z_l is the lateral coordination number, *V* is the same regular solid solution parameter as in KMC, and also similarly to the KMC model, *M* measures the diffusion asymmetry. Here $m' = -2ZM/kT \log_{10} e$, where $Z = 2z_v + z_l$ [25].

Note that in a homogeneous alloy $\alpha = 2ZMc$ and $\varepsilon = 0$, i.e. the activation energy is proportional to the composition.

The input parameters in the model are, therefore [25]: *V* regular solid solution parameter; *T* temperature; z_v, z_l vertical and lateral coordination numbers [$z_v = 4$, $z_l = 0$ for a BCC structure and $z_v = 4$, $z_l = 4$ for an FCC structure in (100) direction]; and m' diffusion asymmetry parameter.

Appendix C. Evaluation

The simulations started form initially homogeneous solid solution matrixes involved multiple stable precipitates and subcritical, unstable nuclei. To identify and count them, the following algorithm was used [34]:

- if a minority (*A*) atom has at least *n* ($n = 3$ in BCC, $n = 4$ in FCC structures) minority neighbours, the atoms form a nucleus;

- a new minority atom is added to a nucleus if it has at least 2 minority neighbours form the nucleus.

Note that in the case when a single spherical nucleus was put into a homogeneous solid solution matrix, we used the same algorithm to determine its evolution in size.

To plot the data in a histogram, the size of the nuclei was grouped into logarithmically spaced bins. Each decade was divided into twenty bins. The frequency was calculated as the total number of the given sized nuclei divided by the bin length [35].

References

[1] Web of science. -. "Nucleation and growth" expression in abstracts.
[2] Sayle, D.C.. J Mater Chem 1998;8:2025.
[3] Sayle, D.C., Richard, C., Catlow, A., Harding, J., Healy, M., Maicaneanu, S., et al. J Mater Chem 2000;10:1315.
[4] Gasser, U., Weeks, E.R., Schofield, A., Pusey, P.N., Weitz, D.A.. Science 2001;292:258.
[5] Pan, D., Wang, Q., An, L.. J Mater Chem 2009;19:1063.
[6] Swaminathan, R., Willard, M., McHenry, M.. Experimental observations and nucleation and growth theory of polyhedral magnetic ferrite nanoparticles synthesized using an rf plasma torch. Acta Materialia 2006;54(3):807 – 816.
[7] Offerman, S.E., van Wilderen, L.J.G.W., van Dijk, N.H., Sietsma, J., Rekveldt, M.T., van der Zwaag, S.. In-situ study of pearlite nucleation and growth during isothermal austenite decomposition in nearly eutectoid steel. Acta Materialia 2003;51(13):3927 – 3938.
[8] Perez, M., Dumont, M., Acevedo-Reyes, D.. Implementation of classical nucleation and growth theories for precipitation. Acta Materialia 2008;56(9):2119 – 2132.
[9] Perez, M., Dumont, M., Acevedo-Reyes, D.. Corrigendum to "implementation of classical nucleation and growth theories for precipitation" [acta materialia 56 (2008) 2119-2132]. Acta Materialia 2009;57(4):1318 – 1318.
[10] Schmaltzried, H.. Chemical Kinetics of Solids. VCH Publ. New York; 1995.
[11] Kashchiev, D.. Nucleation: Basic Theory with Applications. Butterworth-Hainemann, Oxford; 2000.
[12] Cahn, R.W., Haasen, P., editors. Physical Metallurgy. Amsterdam: North Holland; 4th ed.; 1996. P. 688.
[13] ter Host, J.H., Kashchiev, D.. J Chem Phys 2003;119:2241.
[14] ter Host, J.H., Jansen, P.J.. Surf Sci 2005;574:77.
[15] Nishioka, K.. Kinetic and thermodynamic definitions of the critical nucleus in nucleation theory. Phys Rev E 1995;52(3):3263–3265. doi: 10.1103/PhysRevE.52.3263.
[16] Mehrer, H., editor. Diffusion in Solid Metals and Alloys; vol. III/26 of *Landolt-Börnstein, New Series*. Berlin: Springer-Verlag; 1990.
[17] Martin, G.. Atomic mobility in cahn's diffusion model. Phys Rev B 1990;41(4):2279–2283.
[18] Erdélyi, Z., Beke, D.L., Nemes, P., Langer, G.A.. Phil Mag A 1998;79:1757.
[19] Erdélyi1, Z., Sladecek, M., Stadler, L.M., Zizak, I, Langer, G.A., Kis-Varga, M., et al. Science 2004;306:1913.

[20] Erdélyi, Z., Szabó, I.A., Beke, D.L.. Interface sharpening instead of broadening by diffusion in ideal binary alloys. Phys Rev Lett 2002;89(16):165901.

[21] Erdélyi, Z., Beke, D.L., Taranovskyy, A.. Dissolution and off-stoichiometric formation of compound layers in solid state reactions. Applied Physics Letters 2008;92(13):133110 (pages 2).

[22] Balogh, Z., Erdélyi, Z., Beke, D.L., Langer, G.A., Csik, A., Boyen, H.G., et al. Transition from anomalous kinetics toward fickian diffusion for si dissolution into amorphous ge. Applied Physics Letters 2008;92(14):143104 (pages 3).

[23] Katona, G.L., Erdélyi, Z., Beke, D.L., Dietrich, C., Weigl, F., Boyen, H.G., et al. Experimental evidence for a nonparabolic nanoscale interface shift during the dissolution of ni into bulk au(111). Phys Rev B 2005;71(11):115432.

[24] Erdélyi, Z., Katona, G.L., Beke, D.L.. Nonparabolic nanoscale shift of phase boundaries in binary systems with restricted solubility. Phys Rev B 2004;69(11):113407.

[25] Erdélyi, Z., Beke, D.L.. Importance the proper choice of transition rates in kinetic simulation of dynamic processes. Phys Rev B 2004;70:245428.

[26] Soisson, F., Barbu, A., Martin, G.. Monte carlo simulations of copper precipitation in dilute iron-copper alloys during thermal ageing and under electron irradiation. Acta Materialia 1996;44(9):3789 – 3800.

[27] Borchers, J.A., Dura, J.A., Unguris, J., Tulchinsky, D., Kelley, M.H., Majkrzak, C.F., et al. Observation of antiparallel magnetic order in weakly coupled co/cu multilayers. Phys Rev Lett 1999;82(13):2796–2799.

[28] Zahn, P., Binder, J., Mertig, I., Zeller, R., Dederichs, P.H.. Origin of giant magnetoresistance: Bulk or interface scattering. Phys Rev Lett 1998;80(19):4309–4312.

[29] Baibich, M.N., Broto, J.M., Fert, A., Van Dau, F.N., Petroff, F., Etienne, P., et al. Giant magnetoresistance of (001)fe/(001)cr magnetic superlattices. Phys Rev Lett 1988;61(21):2472–2475.

[30] Caro, A., Caro, M., Lopasso, E.M., Crowson, D.A.. Appl Phys Lett 2006;89/12:121902.

[31] Klueh, R.L., Nelson, A.T.. J Nucl Mater 2007;371:37.

[32] Jmol. -. Cteated by Jmol: an open-source Java viewer for chemical structures in 3D. http://www.jmol.org/.

[33] Setna, R.P., Cerezo, A., Hyde, J.M., Smith, G.D.W.. Appl Surf Sci 1994;76-77:203.

[34] Mirold, P., Binder, K.. Acta Metall 1977;25:1435.

[35] Spasojević, D., Bukvić, S., Milošević, S., Stanley, H.E.. Barkhausen noise: Elementary signals, power laws, and scaling relations. Phys Rev E 1996;54(3):2531–2546.